Available online at www.sciencedirect.com

SciVerse ScienceDirect

Journal of the European Ceramic Society 32 (2012) 2423–2430

www.elsevier.com/locate/jeurceramsoc

# Effects of $Ta^{5+}$ doping on microstructure evolution, dielectric properties and electrical response in $CaCu_3Ti_4O_{12}$ ceramics

Prasit Thongbai [a,b,*], Jutapol Jumpatam [a], Teerapon Yamwong [c], Santi Maensiri [d]

[a] *Materials Science and Nanotechnology Program, Faculty of Science, Khon Kaen University, Khon Kaen, 40002, Thailand*
[b] *Integrated Nanotechnology Research Center (INRC), Department of Physics, Faculty of Science, Khon Kaen University, Khon Kaen, 40002, Thailand*
[c] *National Metal and Materials Technology Center (MTEC), Thailand Science Park, Pathumthani, 12120, Thailand*
[d] *School of Physics, Institute of Science, Suranaree University, Nakhon Ratchasima, 30000, Thailand*

Received 18 January 2012; received in revised form 26 February 2012; accepted 28 February 2012
Available online 21 March 2012

**Abstract**

The effects of $Ta^{5+}$ substitution on the microstructure, electrical response of grain boundary, and dielectric properties of $CaCu_3Ti_4O_{12}$ ceramics were investigated. The mean grain size decreased with increasing $Ta^{5+}$ concentration, which was ascribed to the ability of $Ta^{5+}$ doping to inhibit grain boundary mobility. This can decrease dielectric constant values. Grain boundary resistance and potential barrier height of $CaCu_3Ti_4O_{12}$ ceramics were reduced by doping with $Ta^{5+}$. This results in enhancement of dc conductivity and the related loss tangent. Influence of charge compensations on microstructure and intrinsic electrical properties of grain boundaries resulting from the effects of replacing $Ti^{4+}$ with $Ta^{5+}$ are discussed. The experimental data and variation caused by the substitution of $Ta^{5+}$ can be described well by the internal barrier layer capacitor model based on space charge polarization at the grain boundaries.


*Keywords:* Grain growth; Grain boundaries; Dielectric properties; Electrical properties; Capacitors

## 1. Introduction

$CaCu_3Ti_4O_{12}$ (CCTO), a lead-free giant dielectric and non-ferroelectric material, has attracted considerable attention since its anomalous dielectric response was first reported by Subramanian et al.[1] Their discovery stimulated research in the field of high-permittivity materials in recent years. This is for two main reasons. First, CCTO has high potential for use in many electronic applications such as capacitors, memory devices, gas sensors, humidity sensors, and varistors.[1–6] Second, for purely academic reasons, the mechanism of an anomalous dielectric response and the origin of *n*-type semiconductivity of grains are still not clear. This needed to be elucidated. Several models and explanations have now been proposed to clarify these phenomena.[3,7–12]

It is now widely accepted that the giant dielectric response in CCTO ceramics is attributed to an extrinsic effect. The internal barrier layer capacitor (IBLC) effect is based on interfacial polarization (also known as Maxwell–Wagner polarization) at grain boundaries (GBs). It is quite widely accepted as the origin of giant dielectric response in CCTO ceramics.[3,4,6,7] According to the IBLC model, dielectric response in polycrystalline ceramics is due to a special electrically heterogeneous microstructure, consisting of insulating GBs and conductive grains. Changes in electrical properties of GB can cause large changes in the material's dielectric properties. In the other words, if the giant dielectric response in a polycrystalline ceramic results from polarization at GBs, variations of dielectric properties are related to changes in electrical properties in GB regions.

In addition to their giant dielectric properties, CCTO ceramics can also exhibit non-linear electrical behavior. The form of this behavior is seen as a nonlinear relationship between current density ($J$) and electric field ($E$).[4,13–20] This behavior was also observed in other related-perovskite oxides such as $Na_{1/2}La_{1/2}Cu_3Ti_4O_{12}$ ceramics.[21] The cause of this behavior is the existence of intrinsic potential barriers at the GBs, i.e. the Schottky barrier.[4,12] This special behavior originates in the

* Corresponding author at: Materials Science and Nanotechnology Program, Faculty of Science, Khon Kaen University, Khon Kaen, 40002, Thailand. Tel.: +66 84 4190266; fax: +66 43 202374.
*E-mail addresses:* prasitphysics@hotmail.com, pthongbai@kku.ac.th (P. Thongbai).

0955-2219/$ – see front matter © 2012 Elsevier Ltd. All rights reserved.
doi:10.1016/j.jeurceramsoc.2012.02.048

GB regions just as its giant dielectric behavior. Therefore, data obtained from nonlinear *J–E* behavior of CCTO ceramics is strongly related to the electrical properties of GBs and the overall dielectric response.

To clarify the origin of the giant dielectric response and to improve electrical properties of CCTO ceramics, the influences of doping ions substituted into $Ca^{2+}$, $Cu^{2+}$, $Ti^{4+}$, and $O^{2-}$ sites in CCTO crystal lattices have been extensively investigated.[5–7,14,16,18,19,22–33] Most substitution ions have significant effects on the values of dielectric permittivity ($\varepsilon'$), loss tangent ($\tan\delta$), electrical conductivity of GBs ($\sigma_{gb}$), and activation energies for conduction processes at both the GBs ($E_{gb}$) and inside the grains ($E_b$). They also show a great impact on some important behaviors such as dielectric relaxation behavior, bulk nonlinear *J–E* characteristics, and microscopic *J–E* characteristics at individual GBs. Unfortunately, complete research data from published literature for every type of doping ion substitution in CCTO ceramics has not been developed. To obtain more and new data, systematic investigation of electrical and dielectric properties of CCTO ceramics complimenting data of previous work is very important. These studies will give us more understanding of the physical mechanism of giant dielectric properties and the relationship between dielectric and electrical responses at GBs.

As previously reported by Chung et al.,[18] doping of CCTO ceramics using $Nb^{5+}$ and $Ta^{5+}$ cations can modify their nonlinear Ohmic properties and the total macroscopic electrical resistivity of GBs ($R_{gb}$). The breakdown voltage obtained from *J–E* curves and $R_{gb}$ decreased with increasing concentration of dopants. By using local microcontact current–voltage measurements, a decrease in the macroscopic values of the breakdown voltage and $R_{gb}$ are attributed to the decrease in microscopic values of the breakdown voltage, measured across individual single GB layers. These measurements indicate that the macroscopic properties of CCTO ceramics are determined by electrical properties of each GB. For the Nb-doped CCTO ceramics, dielectric properties and electrical response at GBs have been reported.[25,27] Unfortunately, the influence of Ta doping ions on the dielectric properties and resulting electrical responses at GBs, as well as the microstructure of CCTO ceramics, have never been reported.

In this work, we systematically investigated the effects of Ta doping ions on the microstructure, dielectric properties, and electrical response at GBs for CCTO ceramics prepared by a solid state reaction method. The results revealed that Ta doping ions have significant influences on microstructure, dielectric response, and electrical properties of GBs. The possible mechanisms related to these observations are discussed.

## 2. Experimental

In this work, $CaCu_3Ti_{4-x}Ta_xO_{12}$ ceramics, where $x = 0$, 0.02, and 0.04, were prepared by the conventional solid state reaction method. These materials are referred to as CCTO, CCTTO-1 and CCTTO-2, respectively. $CaCO_3$ (99.95% purity), CuO (99.9% purity), $TiO_2$ (99.9% purity), and $Ta_2O_5$ (99.99% purity) were used as starting raw materials. Each stoichiometric mixture of the starting materials was ball-milled in ethanol for 24 h. The mixed slurries were dried and then calcined at 900 °C for 15 h. The calcined powders were ground and pressed into pellets of 9.5 mm in diameter and ~1 mm in thickness by a uniaxial compression at 200 MPa. Finally, these pellets were sintered at 1100 °C for 5 h.

X-ray diffraction (XRD) (Philips PW3040, The Netherlands) and scanning electron microscopy (SEM) (LEO 1450VP, UK) were used to characterize the phase composition and microstructure of the sintered CCTO and Ta-doped CCTO ceramics. Energy dispersive spectroscopy (EDS) (JEOL 5410, UK) was used to investigate the chemical compositions of the polished ceramic samples. Valence states of cations in CCTO and Ta-doped CCTO ceramics were investigated using X-ray photoelectron spectroscopy (XPS) (AXIS Ultra DLD, UK). The dielectric response of the samples was measured using an Agilent E4980A Precision LCR Meter over the frequency and temperature ranges of $10^2$–$10^6$ Hz and −70 to 150 °C, respectively. An oscillation voltage of 500 mV was used in each case. Each temperature was held constant with an accuracy of ±1 °C. Current–voltage measurements were made using a high voltage measurement unit (Keithley Model 247). Prior to measurements, Au was sputtered on each pellet face at a current of 25 mA for 8 min using a Polaron SC500 sputter coating unit.

The complex impedance ($Z^*$) was calculated from the relation,

$$\varepsilon^* = \varepsilon' - j\varepsilon'' = \frac{1}{j\omega C_0 Z^*} = \frac{1}{j\omega C_0 (Z' - jZ'')}, \quad (1)$$

where $\varepsilon'$ and $\varepsilon''$ are, respectively, the real (dielectric constant) and imaginary parts (dielectric loss) of the complex permittivity ($\varepsilon^*$). $Z'$ and $Z''$ are the real part and imaginary part of $Z^*$, respectively. $\omega$ is the angular frequency ($\omega = 2\pi f$) and $j = \sqrt{-1}$. $C_0 = \varepsilon_0 S/d$ is the empty cell capacitance, where $S$ is the sample area, $d$ is the sample thickness, and $\varepsilon_0$ is the permittivity of free space, $\varepsilon_0 = 8.854 \times 10^{-12}$ F/m.

## 3. Results and discussion

Phase formation and crystal structure of the sintered CCTO and Ta-doped CCTO ceramics were studied using an XRD technique (does not presented). The main phase of $CaCu_3Ti_4O_{12}$ was detected in all ceramics without any impurity phases. Fig. 1 shows the surface morphologies of the sintered ceramic samples, revealing grain and grain boundary structures. $Ta^{5+}$ substitution for $Ti^{4+}$ can cause a great change in the microstructure of CCTO ceramics. The mean grain size decreases significantly with increasing Ta dopant content. $Ta^{5+}$ doping ions reduce the grain growth rate of CCTO ceramics. This result is similar to that observed in CCTO ceramics doped with $Nb^{5+}$ cations.[25,27]

Fig. 2(a) and (b) shows EDS spectra for CCTO ceramics measured at grain and GB regions, respectively. Two measured points on the CCTO surface are shown in Fig. 2(c). It was observed in some regions on the CCTO surface, especially for the region shown in Fig. 2(c), that CuO phase is segregated along the GB regions. This is confirmed by a relatively high Cu peak measured in the GB region, as shown in Fig. 2(b). At high sintering

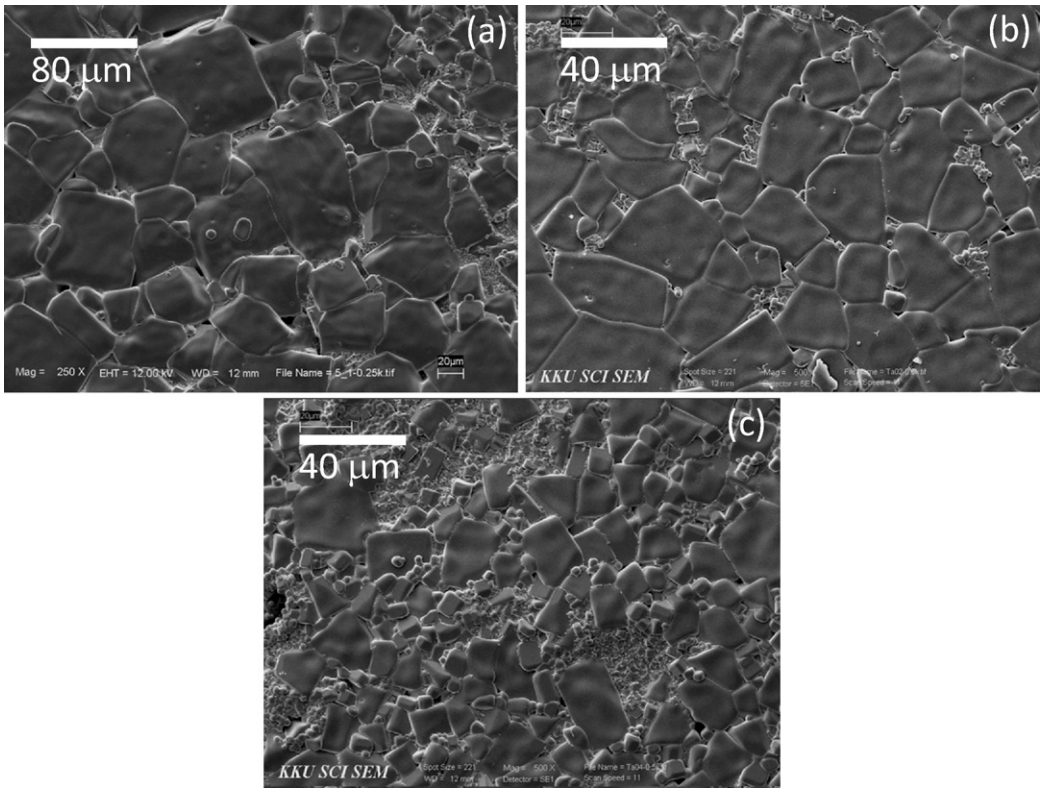


Fig. 1. SEM images of surface morphologies of (a) CCTO, (b) CCTTO-1, and (c) CCTTO-2 ceramic samples.

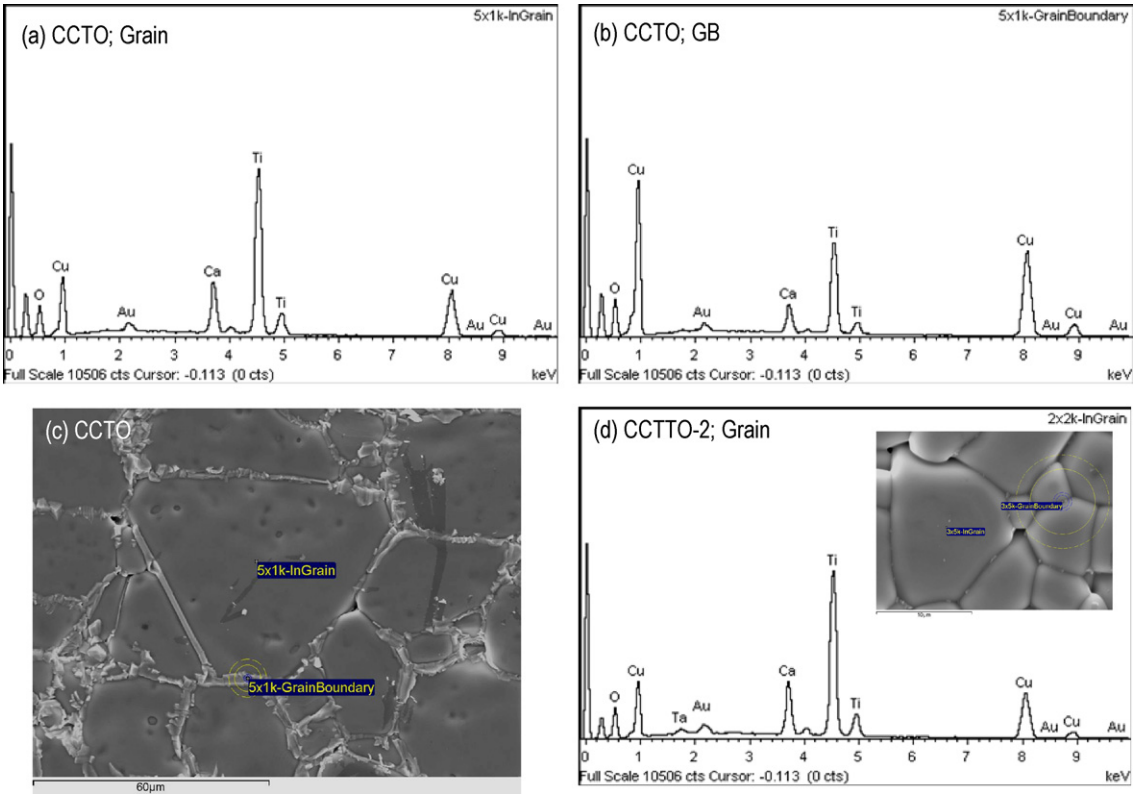


Fig. 2. EDS spectra of (a) CCTO sample detected in grain region, (b) CCTO sample detected at GB region, (c) SEM image of CCTO's surface, and (d) EDS spectrum of CCTTO-2 sample detected in grain region; inset of (d) shows the surface morphology of the CCTTO-2 sample.

temperatures, Cu can be removed from the CCTO. Fig. 2(d) shows the EDS spectrum of the CCTTO-2 sample measured in the grain region. The peak corresponding to Ta is observed in the EDS spectrum of the CCTTO-2 sample. This indicates incorporation of $Ta^{5+}$ ions into the CCTO structure. No evidence of Cu-rich boundary was observed in the EDS spectrum measured at the GB region for the CCTTO-2 sample (does not show).

In general, the grain growth in ceramics is primary driven by GB mobility. This is controlled by the diffusion of ions, atoms, and/or charge species of the grain across the GB. It is reported that the sintering process of CCTO ceramics is associated with the liquid phase sintering mechanism.[34] During the heating process, CuO is a source of a liquid phase, which can increase the densification rate and grain boundary mobility through enhanced matter transport across the GBs. The appearance of a very large mean grain size in the undoped-CCTO sample [Fig. 1(a)] is therefore attributed to the high mobility of GBs. Dopants can often serve several functions during the sintering process, resulting in both kinetic and thermodynamic factors. As shown in Fig. 1(b) and (c), the decrease in grain size of Ta-doped CCTO ceramics may be due to a reduced GB mobility. It is likely that a major role of $Ta^{5+}$ doping ions is their ability to inhibit GB mobility. This observation of $Ta^{5+}$ doped CCTO ceramics is similar to that observed in $Nb^{5+}$ doped $BaTiO_3$ ceramics, which was described in terms of the defect chemistry and space-charge concept.[35] According to the GB model proposed by Chiang and Takagi,[36] electrons and Ti vacancies are expected to accumulate in the negative space charge region. Above the doping threshold, the accumulated Ti vacancies in the space charge may be correlated with a depletion of oxygen vacancies. The diffusivity of oxygen ions ($O^{2-}$) across the GB is very slow due to the relatively large size of $O^{2-}$. This provides a possible mechanism for the significant reduction of GB mobility. In CCTO ceramics, $Ta^{5+}$ substitution for $Ti^{4+}$ requires charge compensation. This can be achieved by one or more of the following mechanisms: (1) filling of oxygen vacancies, (2) decrease of cation valence, (3) creation of cation vacancies, or (4) creation of conduction electrons. It is likely that creation of Ti vacancies and/or conduction electrons may be responsible for the observed decrease in grain size of Ta-doped CCTO ceramics. Furthermore, effective charge compensations can cause changes in the electrical properties and related dielectric response in these ceramics.

Fig. 3(a) demonstrates frequency dependence of $\varepsilon'$ at 30 °C for CCTO and Ta-doped CCTO ceramics. This shows an effect of $Ta^{5+}$ doping ions on $\varepsilon'$ of CCTO ceramics. $\varepsilon'$ tends to decrease as Ta concentration is increased. To exclude the possible effect of sample–electrode contact, the values of $\varepsilon'$ are presented in the low temperature of −70 °C, as shown in Fig. 3(b). A plateau of $\varepsilon'$ values is observed at frequencies below $10^5$ Hz for all samples without an apparent increase in $\varepsilon'$ at frequencies below $10^3$ Hz. A low-frequency plateau of $\varepsilon'$ decreases with increasing concentration of Ta dopant. This indicates that substitution of $Ta^{5+}$ can cause a decrease in primary polarization in CCTO ceramics. Based on the IBLC effect, this decrease in $\varepsilon'$ is attributed to reduction in the intensity of interfacial (space charge) polarization at GBs. Under an applied electric field, interfacial polarization is generally produced at the surfaces of an

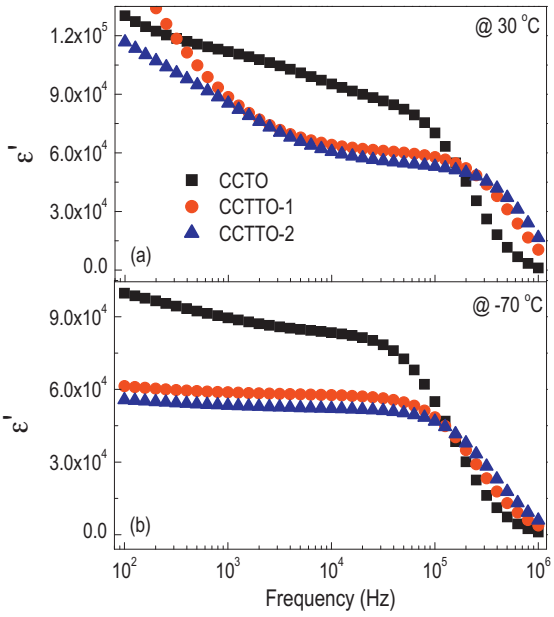


Fig. 3. Frequency dependence of $\varepsilon'$ at (a) 30 °C and (b) −70 °C for CCTO and Ta-doped CCTO ceramics.

insulating GB sandwiched between two semiconducting grains, acting as a micro-parallel plate capacitor. Therefore, the capacitance of a GB ($C_{gb}$) decreases as the grain size is decreased. It is worth noting that the substitution of $Ta^{5+}$ has not only a great influence on the microstructure of the CCTO ceramics, but also a significant effect on their dielectric properties. It is observed that $\varepsilon'$ decreases with decreasing mean grain size. Such dielectric behavior is similar to that observed in undoped-CCTO ceramics.[12,13] By considering only the relationship of $\varepsilon'$ and grain size, it is likely that the decrease in $\varepsilon'$ for Ta-doped CCTO ceramics may be explained by the IBLC model,[34,37]

$$\varepsilon'_{eff} = \frac{\varepsilon_{gb} S}{t_{gb}}, \tag{2}$$

where $\varepsilon'_{eff}$, $\varepsilon_{gb}$, $S$, and $t_{gb}$ are the effective dielectric constant, dielectric constant of the GB, an average grain size, and the thickness of GB, respectively. In this case, reduction of grain size may be a primary cause of the decrease in $\varepsilon'$. However, this result is still insufficient to explain the origin of dielectric response in CCTO ceramics. Variations of other parameters caused by $Ta^{5+}$ substitution need to be suitably modeled.

As shown in Fig. 3, a decrease in $\varepsilon'$ in the high-frequency range is seen. It shifted to slightly higher frequencies as the concentration of Ta dopant was increased. To study the effect of $Ta^{5+}$ substitution on dielectric relaxation behavior in CCTO ceramics, the frequency dependence of $\varepsilon'$ at various low-temperatures was investigated. As shown in Fig. 4 for the CCTTO-1 ceramic, thermally activated dielectric relaxation is observed. The step-like decrease in $\varepsilon'$ and relaxation peak ($\varepsilon''$ peak) shift to low frequency with decreasing temperature. Normally, the dielectric relaxation in CCTO-based ceramics can be empirically

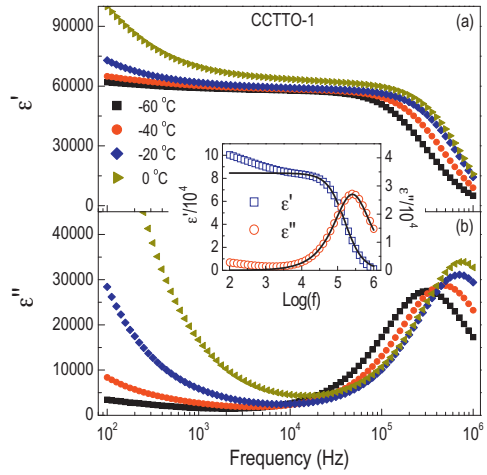


Fig. 4. Frequency dependence of (a) $\varepsilon'$ and (b) $\varepsilon''$ at different temperatures for CCTTO-1 ceramic. Inset shows experimental and fitting results at −70 °C for CCTTO-1 ceramic; the solid curves represent fitting of Eq. (3).

described well by the modified Debye relaxation model, i.e. the Cole–Cole model.[8,13,24,31] This is given by:

$$\varepsilon^* = \varepsilon' - j\varepsilon'' = \varepsilon_\infty + \frac{\varepsilon_s - \varepsilon_\infty}{1 + (j\omega\tau)^{1-\alpha}}, \quad (3)$$

where $\varepsilon_s$ and $\varepsilon_\infty$ are the limiting values of the real part of the permittivity for frequencies below and above the relaxation frequency, $\tau$ is the average relaxation time, and $\alpha$ is constant value representing the distribution of relaxation times. As shown in the inset of Fig. 4, both $\varepsilon'$ and $\varepsilon''$ can be well fitted by the Cole–Cole model. Values of $\alpha$ obtained in this manner were in the range of 0.04–0.05 for all samples. Using the fitted results, values of $\tau$ at different temperatures for all samples were achieved and followed the Arrhenius law,

$$\tau = \tau_0 \exp\left(\frac{E_a}{k_B T}\right), \quad (4)$$

where $\tau_0$ is the pre-factor, $E_a$ is the activation energy required for relaxation process, $k_B$ is Boltzmann constant, and $T$ is absolute temperature. The data fitted using Eq. (4) are presented in Fig. 5. The $E_a$ values for the CCTO, CCTTO-1, and CCTTO-2 samples were found to be 0.086 eV, 0.088 eV, and 0.088 eV,

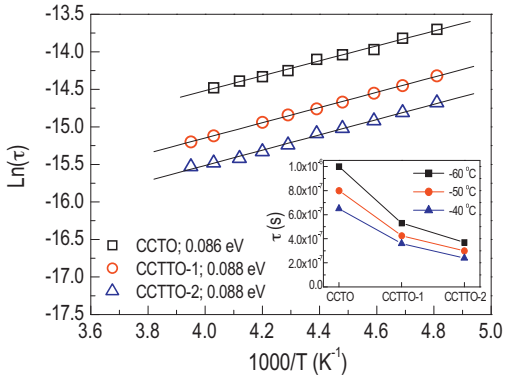


Fig. 5. Arrhenius plots of relaxation time ($\tau$) data for CCTO and Ta-doped CCTO ceramics; inset shows the influence of Ta doping on relaxation time ($\tau$) at selected temperatures.

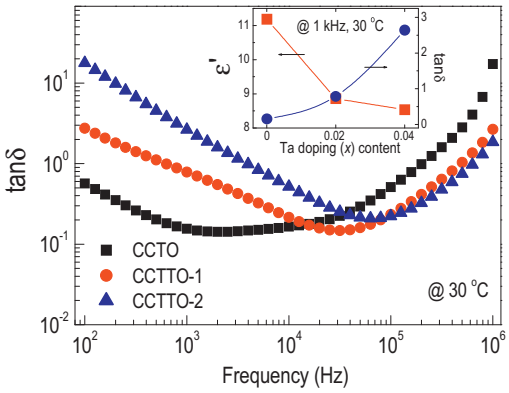


Fig. 6. Frequency dependence of tan $\delta$ at 30 °C for CCTO and Ta-doped CCTO ceramics; inset shows an effect of Ta doping content on the values of $\varepsilon'$ and tan $\delta$.

respectively. These values are comparable to reported values of 0.098–0.116 eV,[13] 0.102 eV,[24] 0.101 eV,[28] 0.103 eV,[31] and 0.011–0.012 eV.[38] Substituting $Ta^{5+}$ dopant for $Ti^{4+}$ has no effect on the activation energy of CCTO ceramics. However, it has an impact on the average relaxation time of electric dipole moment, as shown in the inset of Fig. 5. At a certain temperature, $\tau$ decreases with increasing $Ta^{5+}$ content.

Fig. 6 shows the frequency dependence of tan $\delta$ at 30 °C for CCTO and Ta-doped CCTO ceramics. The increase in tan $\delta$ in a high frequency range for all samples is normally due to the effect of dielectric relaxation process, as is clearly shown in Fig. 4. A high value of tan $\delta$ in a low-frequency range is usually associated with dc conduction processes.[7,37] In a low-frequency range, the relationship between tan $\delta$ and dc conductivity ($\sigma_{dc}$) is estimated as,

$$\tan\,\delta \approx \frac{\sigma_{dc}}{\omega\varepsilon_0\varepsilon_s}. \quad (5)$$

As is shown in Fig. 6, a low-frequency tan $\delta$ increases significantly with increasing Ta doping content, indicating enhancement of dc conductivity in Ta-doped CCTO ceramics. This means that the total resistance of CCTO ceramics, which is governed by the total resistivity of GBs ($R_{gb}$), was reduced by substitution of $Ta^{5+}$ ions. Either the geometry factor or intrinsic electrical properties of CCTO ceramics GBs may be affected by $Ta^{5+}$ dopants.

To understand the effect of $Ta^{5+}$ doping on tan $\delta$ values of CCTO ceramics, the electrical properties of grains and GBs were investigated using impedance spectroscopy at different temperatures. In the absence of sample–electrode effect, $R_{gb}$ can be estimated from the diameter of a large semicircular arc on the impedance complex plane plot ($Z^*$) in a low-frequency range.[3,12] If a high-frequency semicircular arc cannot be observed in a measured frequency range, the grain resistivity ($R_b$) is usually estimated from the nonzero intercept on the $Z'$ axis at high frequencies.[3,12] Obviously, $R_{gb}$ greatly decreases as the concentration of dopant is increased, as shown in Fig. 7. $R_b$ is reduced by a factor of 2 (from 100 to 50 Ω cm, see the inset (2) of Fig. 7). These results are similar to that observed in $Nb^{5+}$ doped CCTO ceramics.[25] The inset (1) of Fig. 7 shows $J$–$E$ curves of the CCTO and Ta-doped CCTO ceramics. The

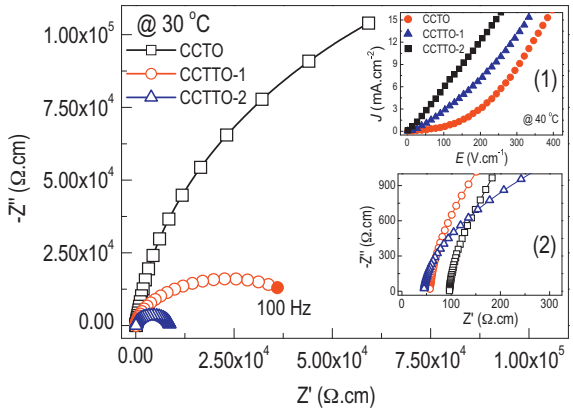


Fig. 7. Impedance complex plane plot ($Z^*$) at 30 °C for CCTO and Ta-doped CCTO ceramic samples. Inset (1) $J$–$E$ curves of CCTO and Ta-doped CCTO ceramics; inset (2) shows an expanded view of the high frequency data close to the origin.

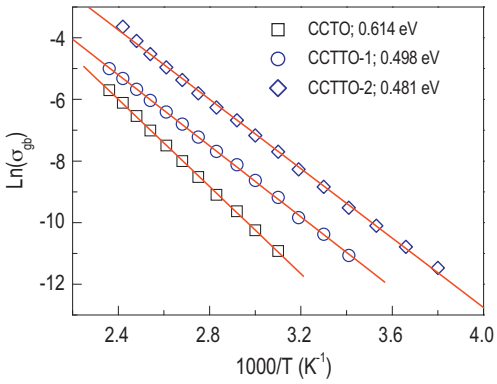


Fig. 8. Arrhenius plots of grain boundary conductivity ($\sigma_{gb}$) data for CCTO and Ta-doped CCTO ceramics.

breakdown voltage decreases with increasing the $Ta^{5+}$ content and non-Ohmic behavior becomes linear. The observed reduction of $R_{gb}$ and change in $J$–$E$ curves for Ta-doped CCTO ceramics are very similar to that reported in Ref. 18. In the work,[18] it was shown that the electrostatic potential barrier ($\Phi_B$) of an individual GB of CCTO ceramics could be reduced by doping with $Nb^{5+}$ and $Ta^{5+}$ ions. It decreases with increasing dopant concentration. Decrease in $\Phi_B$ is thought to be the primary cause for the reduction of both $R_{gb}$ and breakdown voltage of CCTO ceramics. Thus, the increase in tan $\delta$ for Ta-doped CCTO ceramics is attributed to the reduction of $R_{gb}$ (increase in $\sigma_{dc}$) and $\Phi_B$.

As shown in the inset of Fig. 5, $\tau$ decreases as the concentration of $Ta^{5+}$ doping is increased. Based on the IBLC electrically structure model, it was shown that $\tau \approx R_b C_{gb}$ and $\varepsilon' \approx C_{gb}/C_0$.[7] Experimental results revealed that both $R_b$ and $\varepsilon'$ (i.e. parameters related to $C_{gb}$) were decreased by substitution of $Ta^{5+}$ for $Ti^{4+}$ ions. Both results can be used to describe the decrease in $\tau$.

According to a brickwork layer model for electroceramics, the resistivity of an individual GB ($R'_{gb}$) of a ceramics is enhanced by reducing the grain size according to the following relationship,

$$R'_{gb} \approx \frac{t_{gb}}{\sigma'_{gb} S}, \tag{6}$$

where $\sigma'_{gb}$ is the intrinsic electrical conductivity of the GB layer. As shown in Fig. 7, the $R_{gb}$ value of Ta-doped CCTO ceramics was greatly reduced even though grain size decreased. Thus, either a large decrease in $t_{gb}$ or dramatic increase in $\sigma'_{gb}$ is responsible for the reduction of $R'_{gb}$, which results in a decrease in the total $R_{gb}$. It is likely that the increasing value of $\sigma'_{gb}$ may be a primary cause of the decreased $R'_{gb}$ (or $R_{gb}$) value. The $\sigma'_{gb}$ value is intrinsic electrical properties of GBs corresponding to the electronic structure of GBs. It was proposed that double (back-to-back) Schottky potential barriers are created at interfaces of GB layers between $n$-type semiconducting grains.[4,12,18] The electron energy-band structure across the GB is equivalent to $n$–$i$–$n$ with acceptor-like interface traps for electrons within the band gap at the boundary regions. This structure results in bending of the conduction band across the GB, producing an effective $\Phi_B$ height in the GB region.[12] Therefore, electrical transport at the GBs may be correlated to electronic structure of GBs, i.e. Schottky potential barriers. This is consistent with results reported in literature.[39] In this work, the conduction activation energy at GBs ($E_{gb}$) and $\Phi_B$ height are nearly the same in value for CCTO ceramics. We found that the macroscopic (total) electrical conductivity of GBs ($\sigma_{gb}$) calculated from $R_{gb}$ values ($\sigma_{gb} = 1/R_{gb}$) at various temperatures follows the Arrhenius law for the conduction process,

$$\sigma_{gb} = \sigma_0 \exp\left(\frac{-E_{gb}}{k_B T}\right), \tag{7}$$

where $\sigma_0$ is pre-exponential term. The values of $E_{gb}$ were calculated from the slope of plots of $\ln \sigma_{gb}$ vs. $1000/T$, as shown in Fig. 8. $E_{gb}$ values for the CCTO, CCTTO-1, and CCTTO-2 samples were found to be 0.614, 0.498, and 0.481 eV, respectively. Interestingly, $E_{gb}$ decreases with increasing concentration of $Ta^{5+}$ doping, indicating a decrease in $\Phi_B$ with increasing concentration of $Ta^{5+}$ doping ions. This result indicates that the electronic structure of GBs for CCTO ceramics is modified by $Ta^{5+}$ doping cations.

As shown in the inset of Fig. 6, $\varepsilon'$ decreases with increasing $Ta^{5+}$ content. However, tan $\delta$ increases with $Ta^{5+}$ content. Generally, reduction of polarization intensity causes $\varepsilon'$ to decrease. These two results can be well described by the IBLC model based upon space charge polarization at GBs as follows. Under applied electric field, higher charge carriers can cross the potential barrier at GBs when $\Phi_B$ height was reduced. The electrical conductivity and related tan $\delta$ value are enhanced by these charge carriers which can move through the low-barrier GBs. On the other hand, only a small amount of charge carriers can be stored at the GBs. Small accumulated charges make the intensity of polarization decrease, resulting in a reduction of $\varepsilon'$.

In the absence of a dc bias, $\Phi_B$ is expressed as,[12]

$$\Phi_B = \frac{qN_s^2}{8\varepsilon_0 \varepsilon' N_d}, \tag{8}$$

where $q$ is the electronic charge, $N_s$ is the acceptor (surface charge), $\varepsilon'$ is the relative permittivity of materials, and $N_d$ is

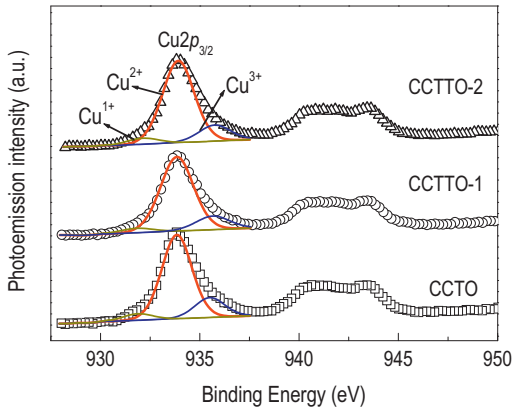


Fig. 9. XPS spectra of CCTO and Ta-doped CCTO ceramics.

the charge carrier concentration in the semiconducting grains. Chung et al.,[18] found that the electrical responses of individual grains are insensitive to $Ta^{5+}$ doping. They proposed that the creation of Ti vacancies caused a decrease in $\Phi_B$, and the number of active acceptor states that contribute to the formation of $\Phi_B$ decreases with increasing $Ta^{5+}$ content. As shown in inset (2) of Fig. 7, $R_b$ decreased with $Ta^{5+}$ cation doping. This indicates an increase in $N_d$, which results in reduction of $\Phi_B$ for Ta-doped CCTO ceramics. As discussed previously, we proposed that the creation of Ti vacancies possibly results from charge compensation of $Ta^{5+}$ substitution, resulting in a decrease in the mean grain size of Ta-doped CCTO ceramics. This is consistent with the results of other researchers.[18] Thus, it is likely that $Ta^{5+}$ substitution is electrically compensated by both the creation of conduction electrons and Ti vacancies. We hypothesize that these two types of charge species have an effect on the potential barrier at GBs of Ta-doped CCTO ceramics. Thus, the decrease in $R_b$ is attributed to the creation of conduction electrons in the grains of Ta-doped CCTO ceramics.

To investigate the oxidation states of polyvalent cations in CCTO and Ta-doped CCTO ceramics, XPS analysis was performed. Fig. 9 shows the XPS spectra of Cu2p regions for all ceramic samples. By using Gaussian–Lorentzian profile fitting, the $2p_{3/2}$ peak for Cu can be divided into three peaks. Major peaks are observed at the binding energies of 933.83, 933.85, and 933.92 eV for CCTO, CCTTO-1, and CCTTO-2 samples, respectively. These peaks correspond to $Cu^{2+}$.[22,40,41] Additionally, the peaks' relatively higher binding energies of 935.48, 935.68, and 935.76 eV, respectively, indicate the presence of $Cu^{3+}$ in these ceramic samples.[22,40] The presence of $Cu^{3+}$ is as observed in Mg-doped CCTO ceramics.[22] Another set of peaks was observed at relatively lower binding energies of 931.99, 931.86, and 932.14 eV for CCTO, CCTTO-1, and CCTTO-2 samples, respectively indicate the presence of $Cu^{+}$.[31,41] The presence of reduced $Cu^{+}$ ions is extensively reported in the literature.[8,24,28,31,41] Quantitative analyses yielding the atomic ratios of $Cu^{2+}/Cu^{3+}/Cu^{+}$ were found to be 1.00/0.25/0.08, 1.00/0.19/0.06, and 1.00/0.20/0.07 for the CCTO, CCTTO-1, and CCTTO-2 samples, respectively. The ratio of $Cu^{3+}/Cu^{2+}$ was reduced by doping with $Ta^{5+}$ ions. The ratio of $Cu^{+}/Cu^{2+}$ was slightly changed.

As seen in Fig. 2, the second phase of CuO was detected at the GBs of the CCTO ceramic sample. It is a decomposition product of $CaCu_3Ti_4O_{12}$ at a high-sintering temperature, producing Cu vacancies. Thus, Cu deficiencies inside the grains lead to the presence of Cu vacancies. To keep the electrical charge balanced, some $Cu^{2+}$ ions were oxidized to $Cu^{3+}$ ions, as observed in XPS spectra in Fig. 9. In the liquid phase sintering mechanism for CCTO ceramics, a liquid phase of Cu is hypothesized to spread throughout the green body during the heating process. It is likely that $Ta^{5+}$ might have some role that inhibits decomposition of Cu during the sintering process. Thus, lower Cu vacancies inside the grains of Ta-doped CCTO ceramics leads to a decrease in $Cu^{3+}$ concentration. It was also found from the XPS spectra that the ratio of $Ti^{3+}/Ti^{4+}$ was reduced by doping with $Ta^{5+}$ ions (does not show). The existence of both $Ti^{3+}$ and $Cu^{+}$ are electrically compensated by the occurrence of oxygen vacancies in ceramics during high-temperature sintering processes. The reduction of $Ti^{3+}/Ti^{4+}$ may be due to the oxidizing property of $Ta^{5+}$. XPS results show that the origin(s) of semiconductivity for CCTO ceramic grains is very complex. The origin of the *n*-type semiconducting grains of CCTO ceramics may be associated with the presence of $Cu^{+}$ and/or $Ti^{3+}$ ions. However, it is still difficult to achieve an accurate explanation of this phenomenon. The presence of these ions in very small amount would be sufficient to induce *n*-type semiconductivity in CCTO ceramics.[34]

## 4. Conclusions

In conclusion, Ta-doped $CaCu_3Ti_4O_{12}$ ceramics were prepared by a conventional solid state reaction method. Their microstructure, dielectric properties, and electrical response of GBs were investigated. Microstructural analysis revealed that $Ta^{5+}$ ions can be incorporated into the structure of $CaCu_3Ti_4O_{12}$. Decrease in the mean grain size was ascribed to the influence of $Ta^{5+}$ ions inhibiting GB mobility. This may cause a decrease in $C_{gb}$, resulting in reduction of $\varepsilon'$. $Ta^{5+}$ doping ions cause $R_{gb}$ and $\Phi_B$ to decrease, resulting in enhancement of $\sigma_{dc}$ and $\tan\delta$. It is likely that $Ta^{5+}$ substitution for $Ti^{4+}$ is electrically compensated by conduction electrons and Ti vacancies. This causes a decrease in $R_b$, $\Phi_B$, and the mean grain size. The values of $\varepsilon'$, $\tan\delta$, $\tau$, $R_{gb}$, $E_{gb}$, and $\Phi_B$ varied with the degree of $Ta^{5+}$ substitution. This can be explained by the IBLC model based on space charge polarization at the GBs. XPS results revealed that oxidation states of Cu, in Ta-doped CCTO ceramics, were found to be +1, +2, and +3 and the oxidation states of Ti were +3 and +4.

## Acknowledgments

J.J. would like to thank the Thailand Graduate Institute of Science and Technology (TGIST) for his Master Degree scholarship. This work was financially supported by the Thailand Research Fund (TRF MRG5480045), the Commission on Higher Education (CHE), and Khon Kaen University, Thailand.

## References


1. Subramanian MA, Li D, Duan N, Reisner BA, Sleight AW. High dielectric constant in $ACu_3Ti_4O_{12}$ and $ACu_3Ti_3FeO_{12}$ phases. *J Solid State Chem* 2000;**151**:323.
2. Home CC, Vogt T, Shapiro SM, Wakimoto S, Ramirez AP. Optical response of high-dielectric-constant perovskite-related oxide. *Science* 2001;**293**:673.
3. Sinclair DC, Adams TB, Morrison FD, West AR. $CaCu_3Ti_4O_{12}$: one-step internal barrier layer capacitor. *Appl Phys Lett* 2002;**80**:2153.
4. Chung SY, Kim ID, Kang SJL. Strong nonlinear current–voltage behaviour in perovskite-derivative calcium copper titanate. *Nat Mater* 2004;**3**:774.
5. Li M, Chen XL, Zhang DF, Wang WY, Wang WJ. Humidity sensitive properties of pure and Mg-doped $CaCu_3Ti_4O_{12}$. *Sens Actuators B* 2010;**147**:447.
6. Kwon S, Huang CC, Patterson EA, Cann DP, Alberta EF, Kwon S, et al. The effect of $Cr_2O_3$, $Nb_2O_5$ and $ZrO_2$ doping on the dielectric properties of $CaCu_3Ti_4O_{12}$. *Mater Lett* 2008;**62**:633.
7. Lunkenheimer P, Krohns S, Fichtl R, Ebbinghaus SG, Reller A, Loidl A. Colossal dielectric constants in transition-metal oxides. *Eur Phys J Special Topics* 2010;**180**:61.
8. Ni L, Chen XM. Dielectric relaxations and formation mechanism of giant dielectric constant step in $CaCu_3Ti_4O_{12}$ ceramics. *Appl Phys Lett* 2007;**91**:122905.
9. Zhu Y, Zheng JC, Wu L, Frenkel AI, Hanson J, Northrup P, et al. Nanoscale disorder in $CaCu_3Ti_4O_{12}$: a new route to the enhanced dielectric response. *Phys Rev Lett* 2007;**99**:037602.
10. Ribeiro WC, Joanni E, Savu R, Bueno PR. Nanoscale effects and polaronic relaxation in $CaCu_3Ti_4O_{12}$ compounds. *Solid State Commun* 2010;**151**:173.
11. Fang TT, Liu CP. Evidence of the internal domains for inducing the anomalously high dielectric constant of $CaCu_3Ti_4O_{12}$. *Chem Mater* 2005;**17**:5167.
12. Adams TB, Sinclair DC, West AR. Characterization of grain boundary impedances in fine- and coarse-grained $CaCu_3Ti_4O_{12}$ ceramics. *Phys Rev B* 2006;**73**:094124.
13. Thongbai P, Putasaeng B, Yamwong T, Maensiri S. Current–voltage nonlinear and dielectric properties of $CaCu_3Ti_4O_{12}$ ceramics prepared by a simple thermal decomposition method. *J Mater Sci Mater Electron* 2012;**23**:795.
14. Luo F, He J, Hu J, Lin YH. Electric and dielectric behaviors of Y-doped calcium copper titanate. *J Am Ceram Soc* 2010;**93**:3043.
15. Lin YH, Cai J, Li M, Nan CW, He J. Grain boundary behavior in varistor-capacitor $TiO_2$-rich $CaCu_3Ti_4O_{12}$ ceramics. *J Appl Phys* 2008;**103**:074111.
16. Leret P, Fernandez JF, de Frutos J, Fernandez-Hevia D. Nonlinear *I–V* electrical behaviour of doped $CaCu_3Ti_4O_{12}$ ceramics. *J Eur Ceram Soc* 2007;**27**:3901.
17. Li T, Xue R, Hao J, Xue Y, Chen Z. The effect of calcining temperatures on the phase purity and electric properties of $CaCu_3Ti_4O_{12}$ ceramics. *J Alloys Compd* 2011;**509**:1025.
18. Chung SY, Choi JH, Choi JK. Tunable current–voltage characteristics in polycrystalline calcium copper titanate. *Appl Phys Lett* 2007;**91**:091912.
19. Ribeiro WC, Araújo RGC, Bueno PR. The dielectric suppress and the control of semiconductor non-Ohmic feature of $CaCu_3Ti_4O_{12}$ by means of tin doping. *Appl Phys Lett* 2011;**98**:132906.
20. Zhang Q, Li T, Chen Z, Xue R, Wang Y. The non-ohmic and dielectric behavior evolution of $CaCu_3Ti_4O_{12}$ after heat treatments in oxygen-rich atmosphere. *Mater Sci Eng B* 2012;**177**:168.
21. Thongbai P, Yamwong T, Maensiri S. Dielectric properties and electrical response of grain boundary of $Na_{1/2}La_{1/2}Cu_3Ti_4O_{12}$ ceramics. *Mater Res Bull* 2012;**47**:432.
22. Li M, Cai G, Zhang DF, Wang WY, Wang WJ, Chen XL. Enhanced dielectric responses in Mg-doped $CaCu_3Ti_4O_{12}$. *J Appl Phys* 2008;**104**:074107.
23. Zhang L, Wu Y, Guo X, Wang Z, Zou Y. Influence of Zr doping on the dielectric properties of $CaCu_3Ti_4O_{12}$ ceramics. *J Mater Sci Mater Electron* 2011, doi:10.1007/s10854-011-0508-5.
24. Ni L, Chen XM, Liu XQ. Structure and modified giant dielectric response in $CaCu_3(Ti_{1-x}Sn_x)_4O_{12}$ ceramics. *Mater Chem Phys* 2010;**124**:982.
25. Liu P, He Y, Zhou JP, Mu CH, Zhang HW. Dielectric relaxation and giant dielectric constant of Nb-doped $CaCu_3Ti_4O_{12}$ ceramics under dc bias voltage. *Phys Status Solidi A* 2009;**206**:562.
26. Zheng Q, Fan H, Long C. Microstructures and electrical responses of pure and chromium-doped $CaCu_3Ti_4O_{12}$ ceramics. *J Alloys Compd* 2012;**511**:90.
27. Hong SH, Kim DY, Park HM, Kim YM. Electric and dielectric properties of Nb-doped $CaCu_3Ti_4O_{12}$ ceramics. *J Am Ceram Soc* 2007;**90**:2118.
28. Ni L, Chen XM. Enhanced giant dielectric response in Mg-substituted $CaCu_3Ti_4O_{12}$ ceramics. *Solid State Commun* 2009;**149**:379.
29. Smith AE, Calvarese TG, Sleight AW, Subramanian MA. An anion substitution route to low loss colossal dielectric $CaCu_3Ti_4O_{12}$. *J Solid State Chem* 2009;**182**:409.
30. Sakamaki R, Cheng B, Cai J, Lin YH, Nan CW, He J. Preparation of $TiO_2$-enriched $CaCu_3Mn_{0.1}Ti_{3.9}O_{12}$ ceramics and their dielectric properties. *J Eur Ceram Soc* 2010;**30**:95.
31. Ni L, Chen XM. Enhancement of giant dielectric response in $CaCu_3Ti_4O_{12}$ ceramics by Zn substitution. *J Am Ceram Soc* 2010;**93**:184.
32. Kim KM, Kim SJ, Lee JH, Kim DY. Microstructural evolution and dielectric properties of $SiO_2$-doped $CaCu_3Ti_4O_{12}$ ceramics. *J Eur Ceram Soc* 2007;**27**:3991.
33. Capsoni D, Bini M, Massarotti V, Chiodelli G, Mozzatic MC, Azzoni CB. Role of doping and CuO segregation in improving the giant permittivity of $CaCu_3Ti_4O_{12}$. *J Solid State Chem* 2004;**177**:4494.
34. Adams TB, Sinclair DC, West AR. Influence of processing conditions on the electrical properties of $CaCu_3Ti_4O_{12}$ ceramics. *J Am Ceram Soc* 2006;**89**:3129.
35. Rahaman MN, Manalert R. Grain boundary mobility of $BaTiO_3$ doped with aliovalent cations. *J Eur Ceram Soc* 1998;**18**:1063.
36. Chiang YM, Takagi T. Grain boundary chemistry of barium titanate and strontium titanate. I: high temperature equilibrium space charge. *J Am Ceram Soc* 1990;**73**:3278.
37. Wu J, Nan CW, Lin YH, Deng Y. Giant dielectric permittivity observed in Li and Ti doped NiO. *Phys Rev Lett* 2002;**89**:217601.
38. Thongbai P, Masingboon C, Maensiri S, Yamwong T, Wongsaenmai S, Yimnirun R. Giant dielectric behaviour of $CaCu_3Ti_4O_{12}$ subjected to post-sintering annealing and uniaxial stress. *J Phys Condens Mater* 2007;**19**:236208.
39. Liu L, Fan H, Fang P, Chen X. Sol–gel derived $CaCu_3Ti_4O_{12}$ ceramics: synthesis, characterization and electrical properties. *Mater Res Bull* 2008;**43**:1800.
40. Yang WZ, Fu MS, Liu XQ, Zhu HY, Chen XM. Giant dielectric response and mixed-valent structure in the layered-ordered double-perovskite ceramics. *Ceram Int* 2011;**37**:2747.
41. Yu R, Xue H, Cao Z, Chen L, Xiong Z. Effect of oxygen sintering atmosphere on the electrical behavior of CCTO ceramics. *J Eur Ceram Soc* 2012;**32**:1245.